

Perspective for aggregation-induced delayed fluorescence mechanism: A QM/MM study

Jie Liu(刘杰), Jianzhong Fan(范建忠), Kai Zhang(张凯), Yuchen Zhang(张雨辰), Chuan-Kui Wang(王传奎), Lili Lin(蔺丽丽)

Citation: Chin. Phys. B . 2020, 29(8): 088504 . **doi:** 10.1088/1674-1056/aba2d9
Journal homepage: http://cpb.iphy.ac.cn; http://iopscience.iop.org/cpb

What follows is a list of articles you may be interested in

Luminescent properties of thermally activated delayed fluorescence molecule with intramolecular *π*-*π* interaction betweendonor and acceptor

Lei Cai(蔡磊), Jianzhong Fan(范建忠), Xiangpeng Kong(孔祥朋), Lili Lin(蔺丽丽), Chuan-Kui Wang(王传奎)
Chin. Phys. B . 2017, 26(11): 118503 . **doi:** 10.1088/1674-1056/26/11/118503

Bias-dependent timing jitter of 1-GHz sinusoidally gated InGaAs/InP avalanche photodiode

Ge Zhu(朱阁), Fu Zheng(郑福), Chao Wang(王超), Zhibin Sun(孙志斌), Guangjie Zhai(翟光杰), Qing Zhao(赵清)
Chin. Phys. B . 2016, 25(11): 118505 . **doi:** 10.1088/1674-1056/25/11/118505

Highly efficient blue fluorescent OLEDs with doped double emitting layers based on p–n heterojunctions

Su Yue-Ju,Wu Xiao-Ming,Hua Yu-Lin,Shen Li-Ying,Jiao Zhi-Qiang,Dong Mu-Sen,Yin Shou-Gen
Chin. Phys. B . 2012, 21(5): 058503 . **doi:** 10.1088/1674-1056/21/5/058503

Perspective for aggregation-induced delayed fluorescence mechanism: A QM/MM study*

Jie Liu(刘杰), Jianzhong Fan(范建忠), Kai Zhang(张凯), Yuchen Zhang(张雨辰), Chuan-Kui Wang(王传奎)†, and Lili Lin(蔺丽丽)‡

Key Laboratory of Medical Physics and Image Processing & Shandong Provincial Engineering and Technical Center of Light Manipulations, School of Physics and Electronics, Shandong Normal University, Jinan 250358, *China*

(Received 2 May 2020; revised manuscript received 23 June 2020; accepted manuscript online 6 July 2020)

To enhance the potential application of thermally activated delayed fluorescence (TADF) molecular materials, new functions are gradually cooperated to the TADF molecules. Aggregation induced emission can effectively solve the fluorescence quenching problem for TADF molecules in solid phase, thus aggregation-induced delayed fluorescence (AIDF) molecules were recently focused. Nevertheless, their luminescent mechanisms are not clear enough. In this work, excited state properties of an AIDF molecule DMF-BP-DMAC [reported in *Chemistry–An Asian Journal* **14** 828 (2019)] are theoretically studied in tetrahydrofuran (THF) and solid phase. For consideration of surrounding environment, the polarizable continuum method (PCM) and the combined quantum mechanics and molecular mechanics (QM/MM) method were applied for solvent and solid phase, respectively. Due to the increase of the transition dipole moment and decrease of the energy difference between the first single excited state (S_1) and the ground state (S_0), the radiative rate is increased by about 2 orders of magnitude in solid phase. The energy dissipation of the non-radiative process from S_1 to S_0 is mainly contributed by low-frequency vibrational modes in solvent, and they can be effectively suppressed in aggregation, which may lead to a slow non-radiation process in solid phase. Both factors would induce enhanced luminescence efficiency of DMF-BP-DMAC in solid phase. Meanwhile, the small energy gap between S_1 and triplet excited states results in high reverse intersystem crossing (RISC) rates in both solvent and solid phase. Therefore, TADF is confirmed in both phases. Aggregation significantly influences both the ISC and RISC processes and more RISC channels are involved in solid state. The enhanced delayed fluorescence should be induced by both the enhanced fluorescent efficiency and ISC efficiency. Our calculation provides a reasonable explanation for experimental measurements and helps one to better understand the luminescence mechanism of AIDF molecules.

Keywords: thermally activated delayed fluorescence, aggregation-induced delayed fluorescence, the combined quantum mechanics and molecular mechanics method

PACS: 85.60.Bt **DOI:** 10.1088/1674-1056/aba2d9

1. Introduction

As the third-generation luminescent materials, thermally activated delayed fluorescence (TADF) emitters have received much attention in recent years, due to their potential application in organic light-emitting diodes (OLEDs) for display and illumination.[1–4] The OLEDs based on TADF emitters, which can make full use of both triplet and singlet excitons via reverse intersystem crossing (RISC), can achieve nearly 100% internal quantum efficiencies (IQE).[5–8] As we all know, most TADF molecules require complex doping techniques to suppress emission quenching and face severe efficiency roll-off, which limits the wild application of TADF molecules.[9,10] The aggregation induced emission (AIE) feature provides a valid strategy for solving this problem of TADF molecules.[11–15] AIE-TADF molecules were designed and synthesized by Tang's group, and most of them were based on substantial inhibition of the twisting of the individual groups in the solid state.[11–14] Besides, Chi's group also reported AIE-TADF molecules using a spatially close donor–acceptor (D–A) interaction with the D and A groups linked to the ortho-position.[15] In addition, Tang's group also innovatively developed a series of aggregation-induced delayed fluorescence (AIDF) molecules which can exhibit strong delayed fluorescence upon aggregate formation, and they are thought as a special kind of AIE-TADF molecules.[14,16–18] Although many studies have explored the AIE mechanism of luminescent molecules, little study focused on the aggregation–delayed fluorescence relationship.[19–22] How does aggregation enhance the delayed fluorescence in AIDF molecules? It is still not clear enough. In this paper, the D-A-D' type molecule (9, 9-dimethyl-9H-fluoren-2-yl) (4-(9,9-dimethylacridin-10-yl)phenyl) methanone (DMF-BP-DMAC) (shown in Fig. 1(a)), which is an AIDF molecule synthesized by Tang's group,[23] is studied as a model system to investigate the DF mechanism theoretically. The excited states properties of DMF-BP-DMAC in both tetrahydrofuran (THF) and solid phases are studied using the polarizable con-

*Project supported by the National Natural Science Foundation of China (Grant Nos. 11874242, 11974216, and 11904210), Shandong Provincial Natural Science Foundation, China (Grant No. ZR2019MA056), Taishan Scholar Project of Shandong Province, China, and the China Postdoctoral Science Foundation (Grant No. 2018M642689).

†Corresponding author. E-mail: ckwang@sdnu.edu.cn

‡Corresponding author. E-mail: linll@sdnu.edu.cn

© 2020 Chinese Physical Society and IOP Publishing Ltd

tinuum model (PCM)[24] and the combined quantum mechanics and molecular mechanics (QM/MM) method[25] respectively. Besides, the decay rates of the excited states are calculated, and the DF mechanism for DMF-BP-DMAC is theoretically elucidated.

2. Theoretical methods and computational details

In our calculation, the PCM is adopted to include the solvent effect on the photophysical properties of the molecule. The geometric and electronic structures for DMF-BP-DMAC in ground state (S_0) are investigated using the density functional theory (DFT). The time-dependent density functional theory (TD-DFT) is adopted for the optimization of the excited states. The molecular configuration is shown in Fig. 1(b). To investigate the properties of DMF-BP-DMAC in solid phase, the QM/MM method with a two-layer ONIOM approach is used.[26–30] The computational model is constructed based on the crystal structures of DMF-BP-DMAC obtained experimentally.[23] The model we used is shown in Fig. 1(c). The two-layer ONIOM method is adopted with one molecule in the center calculated with the QM method and the other molecules surrounded calculated using the MM method. For the QM calculation, the DFT is used to investigate the properties of the ground state and the TD-DFT is adopted to study the properties of the excited states. The MM calculation is treated using the efficient universal force field (UFF) method, and the MM part is frozen during the QM/MM geometry optimizations for the all states. All the calculations above are realized in Gaussian 16 program.[31]

Although TD-DFT method has been widely used for the calculation of excited states especially for organic systems, the properties of excited states were found sensitive to the functionals with different HF proportions (HF%) for different molecules.[32–36] So, several DFT functionals including B3LYP, PBE0, BMK, and M062X were tested (as shown in Table 1). It is found that the emission wavelengths calculated with the PBE0 functional for DMF-BP-DMAC in the THF and solid phase are 542 nm and 517 nm, respectively, which are in good agreement with the experimental values (534 nm in the THF and 510 nm in solid phase). Therefore, the PBE0 functional with 6-31G (d) basis set is adopted in our following calculations.

Table 1. Emission wavelength and oscillator strength calculated by different functionals for DMF-BP-DMAC in tetrahydrofuran (THF) and solid phase.

	THF		Solid	
	λ/nm	f	λ/nm	f
B3LYP	590	0.0001	561	0.0068
PBE0	542	0.0001	517	0.0089
BMK	447	0.0006	430	0.0176
M062X	394	0.0223	396	0.0055
Exp.[a]	534	–	510	–

[a]Exp. is the experimental emission wavelength.

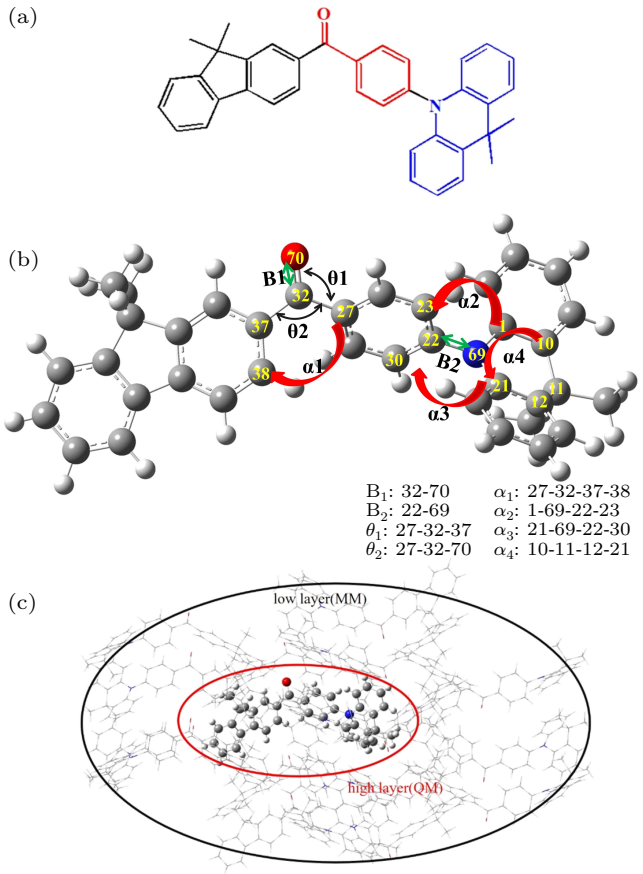


Fig. 1. (a) Chemical structure of DMF-BP-DMAC. (b) The atomic labels and the interesting bond lengths (B_1, B_2), bond angles (θ_1, θ_2), and dihedral angles (α_1, α_2, α_3, and α_4). (c) ONIOM model: surrounding molecules are regarded as low layer and the centered DMF-BP-DMAC is treated as high layer.

Furthermore, the radiative decay rate (K_r) from the first single excited state (S_1) to S_0 can be calculated by Einstein spontaneous emission equation as follows:

$$K_r = \frac{f\Delta E_{fi}^2}{1.499}, \tag{1}$$

where f is the oscillator strength and ΔE_{fi} is the vertical emission energy between the first single excited state (S_1) and the ground state (S) in units of wavenumber (cm^{-1}).[37]

The ISC rate K_{ISC} and RISC rate K_{RISC} between single and triplet excited states can be computed using the classical Marcus rate equation[38]

$$\begin{aligned} K_{ji} &= \frac{V_{ji}^2}{\hbar}\sqrt{\frac{\pi}{K_B T\lambda}}\exp\left[-\frac{(\Delta G_{ji}+\lambda)^2}{4\lambda K_B T}\right] \\ &= \frac{V_{ji}^2}{\hbar}\sqrt{\frac{\pi}{K_B T\lambda}}\exp\left[-\frac{\Delta G^{\perp}}{K_B T}\right]. \end{aligned} \tag{2}$$

Here, K_B is the Boltzmann constant; V_{ji} is the spin–orbit coupling (SOC) between the S_1 state and the triplet excited states (T_n), and it is calculated with the quadratic response function method which can be realized with the Dalton program;[39] ΔG_{ji} is defined as the difference between the adiabatic energies of the final and initial states. In calculation of the ISC rate, $\Delta G_{ji} = E_{S_1} - E_{T_n}$; and for the RISC process, $\Delta G_{ji} = E_{T_n} - E_{S_1}$. T is the temperature and λ is the reorganization energy. For

ISC process, λ_T is the difference between the triplet excited state energy at S_1 geometry and T_n geometry. For the RISC process, λ_S is the gap between the singlet excited state energies at triplet excited state geometry and at the S_1 geometry.[40] Detailed analyses of DMF-BP-DMAC on excited state properties are illustrated in the following sections.

3. Results and discussion

3.1. Geometric structures

Molecular geometry determines both the electronic structures and photophysical properties. Thus, the geometric structures of DMF-BP-DMAC at S_0, S_1, and T_n are theoretically studied in both THF and solid phase. Selected key geometric parameters (marked in Fig. 1(b)) of these structures are compiled in Table 2. It is found that the variations of bond lengths and bond angles are extremely small when the molecule is excited from S_0 to S_1 or T_n. However, the dihedral angles change significantly when the molecules are excited from one state to another. The variations of dihedral angles happened between two states in THF are larger than those in solid phase. Comparing data of the dihedral angles α_1, α_2, and α_3 in THF, significant changes (4.8°, 10.6°, and 9.9°) between S_0 and S_1 are found. The α_4 alters from 39.06° in the S_0 state to 0.20° in the S_1 state. In solid phase, the changes of dihedral angles do not exceed 10°. The action of surrounding molecules in the aggregate state leads to the limitation of the rotation of the dihedral angle of the molecule. In addition, the dihedral angle variations for DMF-BP-DMAC in THF when it is excited from S_0 to T_n are also larger than those in solid phase. In order to quantitatively characterize the change of geometry, the root of the mean of squared displacement (RMSD) is calculated by Multiwfn.[41,42] The geometry changes and the RMSD values are shown in Fig. 2. It is clearly shown that the geometric change between S_0 and S_1 in THF is mainly in two donors, and the value of RMSD is 0.829 Å. However, this value between S_0 and S_1 in solid phase is 0.089 Å, about one tenth of the value in THF. Since the non-radiative process is closely related to the geometric changes during state transition, the non-radiative energy consumption path in solid phase should be different from that in THF. In general, smaller geometric change would induce smaller reorganization energy and slower non-radiative rate, thus suppressed non-radiative process is expected for DMF-BP-DMAC in solid phase. Meanwhile, the variations of geometric structures of S_1 and T_n are heavily interrelated with the ISC and RISC processes, we thus present some comparison of their geometries (shown in Fig. 2). The RMSD between S_1 and T_1 in solid phase is 0.065 Å, which is much smaller than that in THF (RMSD = 0.482 Å). Since T_2 may also contribute to the ISC and RISC processes in the THF, the RMSD of S_1 and T_2 (0.423 Å) is also calculated. In the solid phase, T_2 and T_3 are close to S_1 in energy, thus the values of RMSD between them and S_1 are also calculated (0.062 Å and 0.063 Å). This indicates small reorganization energies for the ISC and RISC processes in the solid phase. Through above careful analysis on geometry, the non-radiative process and ISC process in solid phase are expected to be affected due to the influence of the surrounding environment. Different geometry changes in THF and solid phase are shown to have close relationship with the photophysical properties.

Table 2. Geometry parameters of S_0, S_1, T_1, and T_2 states for DMF-BP-DMAC in THF and those of S_0, S_1, T_1, T_2, and T_3 states for DMF-BP-DMAC in solid phase. Bond lengths (B_1, B_2), bond angles (θ_1, θ_2), and dihedral angles (α_1, α_2, α_3, α_4) are marked in Fig. 1(b).

	THF				Solid				
	S_0	S_1	T_1	T_2	S_0	S_1	T_1	T_2	T_3
B_1	1.23	1.27	1.27	1.27	1.22	1.26	1.26	1.25	1.25
B_2	1.43	1.44	1.43	1.43	1.42	1.45	1.44	1.44	1.44
θ_1	120.39	121.71	121.88	121.71	119.17	119.01	119.50	120.26	120.24
θ_2	119.27	120.20	119.92	120.17	119.96	120.58	120.38	120.05	120.05
α_1	27.62	32.42	32.88	33.71	−40.28	−40.62	−41.10	−34.94	−34.98
α_2	−79.38	−89.98	−67.94	−110.49	75.99	83.60	75.79	78.03	77.98
α_3	81.24	−91.10	−69.22	−111.09	84.53	81.04	73.37	79.48	79.42
α_4	39.06	0.20	−1.88	2.51	−38.53	−33.84	−34.64	−36.44	−36.52

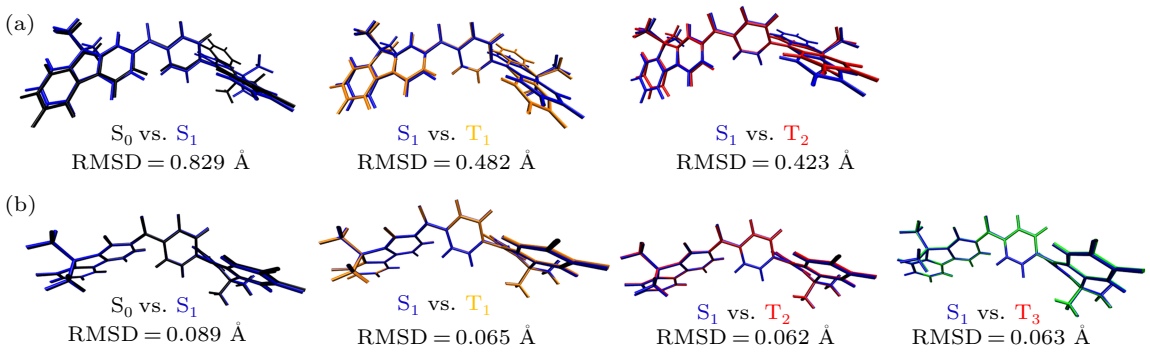


Fig. 2. Geometry changes between two selected states for DMF-BP-DMAC in THF (a) and solid phase (b).

3.2. Energy gap and transition property

For DMF-BP-DMAC, the S_1 state is dominated by the transition from the highest occupied molecular orbital (HOMO) to the lowest unoccupied molecular orbital (LUMO) in both THF and solid phase. The frontier molecular orbitals are shown in Fig. 3. The HOMO is mainly concentrated in the DMAC group, while the LUMO is mainly in the DMF and BP units. The transition properties in solid phase have not changed. Due to the smaller orbital overlap of HOMO–LUMO, the electron exchange energy is smaller, it may lead to the small single and triplet energy gaps in the solvent and solid phase. The energy of HOMO in the THF is −5.48 eV, and the energy of LUMO is −1.95 eV. In the solid phase, the energies of both orbitals increase, the energy of HOMO increases to −5.30 eV, and the energy of LUMO increases to −1.79 eV. Nevertheless, the energy gap between HOMO and LUMO is almost unchanged.

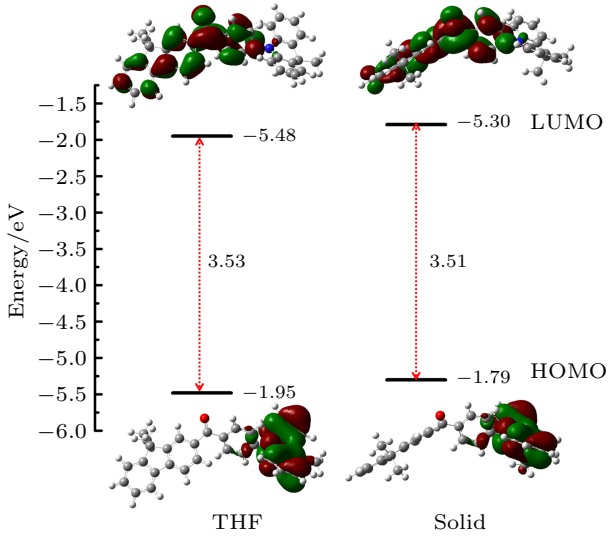


Fig. 3. Energy levels and distributions of HOMO and LUMO for molecule in THF and solid phase (isovalue = 0.02).

The excitation energies calculated based on the optimized geometries of the excited states of DMF-BP-DMAC in THF and solid phase are shown in Figs. 4(a) and 4(b). The calculated energy gap between S_0 and S_1 in solid phase is larger than that in THF. It is the reason that the emission wavelength is blue-shifted in solid phase, which is consistent with the experimental results. It also can be seen that there are two triplet excited states (T_1, T_2) below S_1 in energy, and the energy values of the two triplet excited states are nearly identical in THF. In solid phase, there is only one triplet excited state (T_1) below S_1, and the energy gap is 0.05 eV, which is larger than that in THF (0.03 eV). Although the energy of T_2 and T_3 is higher than that S_1, they are close to each other, with energy gap of 0.14 eV. The efficient RISC process should also happen from T_2, T_3 to S_1. The small energy gap can efficiently favor the RISC processes from the triplet excited states to S_1 in both THF and solid phase and it is indicated that the solid state provides more ISC and RISC channels. The transition properties and SOC between the single and triplet excited states also have important effect on the ISC and RISC processes.

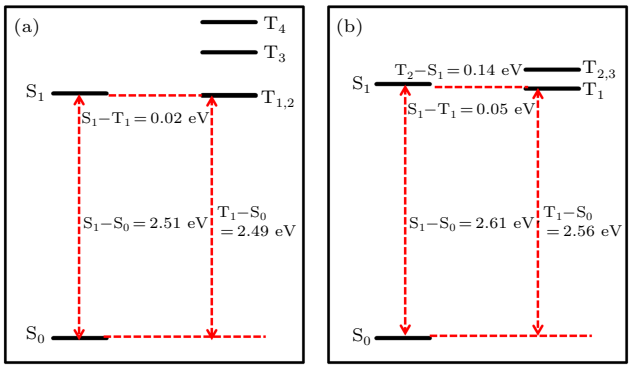


Fig. 4. Adiabatic excitation energies for DMF-BP-DMAC in THF (a) and solid phase (b).

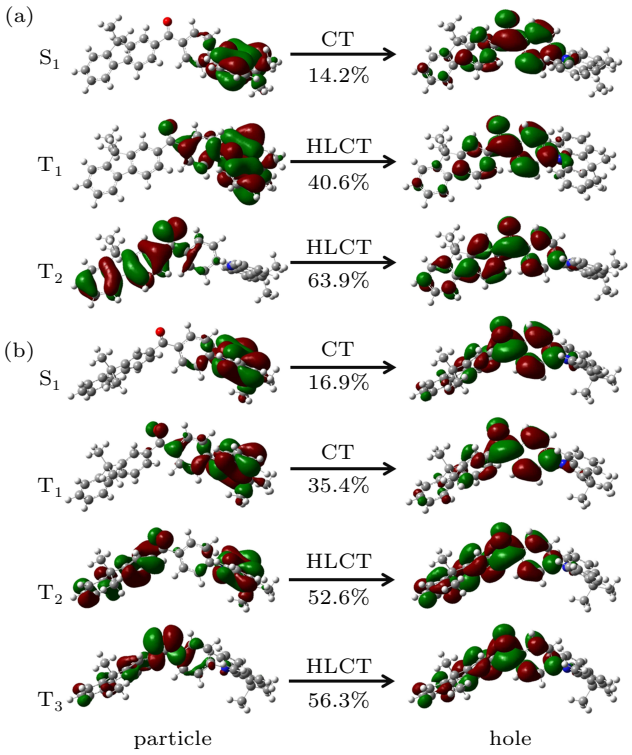


Fig. 5. Transition characteristics for S_1, T_1, and T_2 of DMF-BP-DMAC in THF (a) and transition characteristics for S_1, T_1, T_2, and T_3 of DMF-BP-DMAC in solid phase (b) (isovalue = 0.02). The value below every arrow represents the component of localized excitation in the corresponding transition.

The natural transition orbital (NTO) analyses for S_1, T_1, T_2, and T_3 of DMF-BP-DMAC in THF and solid phase are performed. The particle and hole are shown in Fig. 5. The value below every arrow represents the component of localized excitation in the corresponding transition. According to previous reports, these values can be quantitatively analyzed with a ratio of 0%–40% for the charge transfer (CT) state, a ratio of 40%–75% for the hybridized local charge-transfer (HLCT) state, and a ratio of 75%–100% for the locally excited (LE)

state.[43,44] In THF, we can find that S_1 is a CT state, and T_1 and T_2 are the HLCT states. However, the transition properties of S_1 and T_1 are the CT state in the solid phase. Meanwhile, according to the value of localized excitation, small ΔE_{ST} and different transition characteristic between S_1 and T_n lead to large RISC in THF. In the solid phase, the LE component of T_1 state is 35.4%, the CT states tend to form a small ΔE_{ST}, and the same is true for our calculations. Both T_2 and T_3 are HLCT states, and the LE components for them are 52.6% and 56.3%, respectively. Those also produce small ΔE_{ST} and large SOC, in turn it is beneficial to the production of the RISC process.

3.3. Radiative and non-radiative process

The radiative decay rates are calculated by formula (1). The K_r increases from solution (2.27×10^4 s^{-1} in THF) to solid phase (2.29×10^6 s^{-1}) by about 100 times. The increased radiative rate would be helpful for enhanced fluorescence efficiency in solid phase. In THF, the oscillator strength is 0.0001, and the vertical emission energy between S_1 and S is 2.89 eV. In the solid phase, the oscillator strength has increased to 0.0068, and the energy gap becomes 2.39 eV. Therefore, we can find that the increase of radiative decay rate is mainly due to the increase of oscillator strength, this is caused by the enlarged transition dipole moment for DMF-BP-DMAC in solid phase (0.99D) compared with that in THF (0.39D).

In addition, the non-radiative process is an important aspect of studying photophysical properties. Huang–Rhys (HR) factor is an effective parameter to measure the non-radiative process of excited states. To analyze the non-radiative process, the HR factor is calculated using the DUSHIN program.[45] Under the harmonic oscillator approximation, the HR is expressed as $HR_i = \omega_i D_i^2/2$. In the equation, ω_i denotes the frequency of the i-th normal mode, and D_i is the difference of equilibrium geometries in two electronic states. Then, HR factors versus the normal-mode frequencies in THF and solid phase are drawn in Figs. 6(a) and 6(b). For the decay process in THF, the large HR factors 27.4 (31.1 cm^{-1}), 25.0 (58.8 cm^{-1}), and 16.6 (594.5 cm^{-1}) are corresponding to the vibration of the DMAC part. For the decay process in the solid phase, the large HR factors 0.55 (52.6 cm^{-1}), 0.22 (381.2 cm^{-1}), and 0.18 (437.5 cm^{-1}) are also corresponding to the vibration of the DMAC part. However, the vibration amplitude in the solid phase is much smaller than that in the solvent due to the intermolecular interaction. It indicates the importance of low frequency modes couplings in the non-radiative decay from S_1 to S. It can be seen that the HR factors of DMF-BP-DMAC in solid phase are all smaller by 15 times than those in THF, which indicates that the non-radiative rate in the solid phase would be smaller than that in the THF. Thus the non-radiative energy consumptions of the excited state would be hindered in the solid phase, and the AIE mechanism is expected for DMF-BP-DMAC.

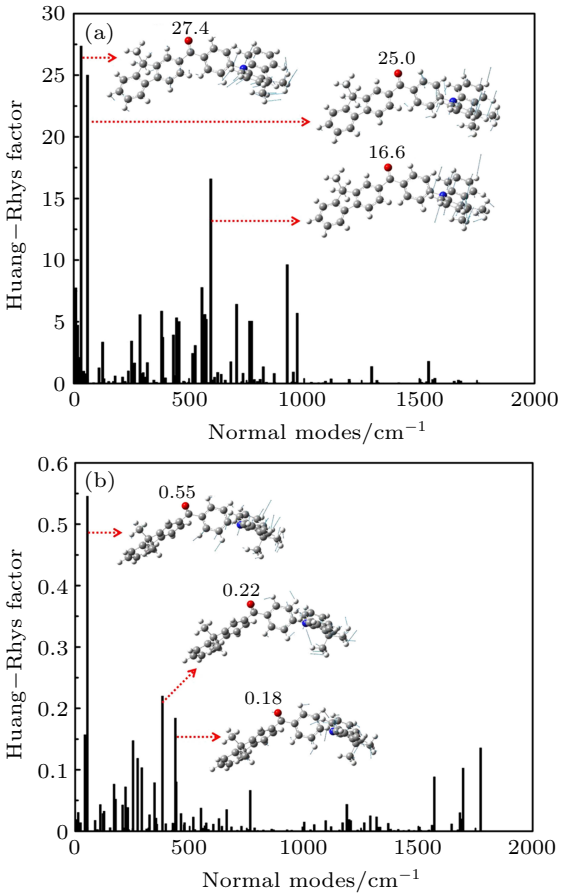


Fig. 6. The calculated HR factors of DMF-BP-DMAC in THF (a) and solid phase (b). The corresponding vibration modes are shown in inset.

3.4. Intersystem crossing and reverse intersystem crossing process

The standards for evaluating effective TADF materials are generally combined with smaller ΔE_{ST} and reasonably fast RISC rates. Qualitatively speaking, large SOC values not only benefit to the ISC process from S_1 and T_n but also the RISC process form T_n to S_1. To determine quantitatively the photophysical processes, according to formula (2), in combination with the electronic structure calculations, the related SOC and associated reorganization energies as well as ISC and RISC rates at room temperature are calculated in THF and solid phase, which are collected in Table 3. In THF, the SOC values between S_1 and T_1 (T_2) are all calculated respectively. The SOC values between S_1 and T_1 (T_2 and T_3) are also calculated in solid phase. The SOC values between S_1 and T_1 at S_1 structure are calculated to be 0.01 cm^{-1} and 0.19 cm^{-1}. The values at T_1 structure are larger than that at S_1 minima (0.44 cm^{-1} and 0.39 cm^{-1}). The SOC value between S_1 and T_2 in THF is 0.67 cm^{-1}, which is larger than that between S_1 and T_1. Simultaneously, the SOC value between S_1 and T_2 at T_2 structure in THF is 1.84 cm^{-1}, which is also larger than that at S_1 structure. In solid phase, the SOC value between S_1 and T_2 at T_2 minima is 0.44 cm^{-1}, which is larger than that at

S_1 minima (0.38 cm^{-1}). The SOC value between S_1 and T_3 at T_3 minima structure is 0.81 cm^{-1}, which is larger than that between S_1 and T_1, T_2. The SOC values between S_1 and triplet state at triplet state minima structure are larger than that at S_1 minima structure. It is indicated that the RISC processes are very likely to happen whether in solvent or solid phase. In addition to the SOC values, reorganization energies are another important factor to regulate the ISC and RISC rates. For the ISC process, the λ_T between S_1 and T_1 is 15.6 meV in THF, which is small than that between S_1 and T_2 (421.1 meV). The λ_T between S_1 and T_1 is also small (24.5 meV) in the solid phase. By contrast, the λ_S between S_1 and T_1, T_2 in THF are similar, which are 124.2 meV and 106.4 meV, respectively. In solid phase, the λ_S between S_1 and T_1 is 52.1 meV. According to formula (2), when the other values are fixed, the smaller the difference between reorganization energy and energy gap between two states, the greater the ISC and RISC rate.

Based on the calculated SOC, λ, and ΔE_{ST} values, in-depth analysis of the calculated K_{ISC} and K_{RISC} of DMF-BP-DMAC in THF is performed. In THF, the K_{RISC} values are always larger than those of K_{ISC}. For example, the ISC rate from S_1 to T_1 is 1.98×10^5 s^{-1}, and the RISC rate from T_1 to S_1 is 1.87×10^{10} s^{-1}. This is due to the large SOC and small λ of the RISC process. The ISC rate from S_1 to T_3 is 2.51×10^7 s^{-1}. It is obvious that the ISC process mainly happens between S_1 and T_2, T_3. The RISC rate from T_3 to S_1 is 2.5 s^{-1} and the RISC process mainly happens between T_1 and S_1. The ISC rate in solid phase (4.81×10^7 s^{-1}) is larger than that in THF and the RISC rate in solid phase (2.68×10^7 s^{-1}) is smaller than that in THF. The ISC rate from S_1 to T_1 in solid phase is 4.81×10^7 s^{-1}. It is larger than the ISC rate from S_1 to T_2 and T_3. The RISC rate from T_2 to S_1 is 1.30×10^8 s^{-1}, and the RISC rate from T_3 to S_1 is 4.40×10^8 s^{-1}. It is larger than the RISC rate from T_1 to S_1 (4.81×10^7 s^{-1}). For the RISC process, T_1, T_2, and T_3 all contribute significantly. Thus more RISC channels are found in solid state than in THF. Both K_{ISC} and K_{RISC} are visibly affected by the SOC, λ, and ΔE_{ST}.

Table 3. Spin–orbit coupling (SOC), reorganization energy (λ), energy difference (ΔE), intersystem crossing rates (K_{ISC}), and reverse intersystem crossing rates (K_{RISC}) between single excited states and triplet excited states.

		SOC[a]/cm^{-1}	SOC[b]/cm^{-1}	λ_S/meV	λ_T/meV	ΔE/meV	K_{ISC}/s^{-1}	K_{RISC}/s^{-1}
THF	S_1–T_1	0.01	0.44	124.2	15.6	24.1	1.98×10^5	1.87×10^{10}
	S_1–T_2	0.67	1.84	106.4	421.1	17.6	4.14×10^6	6.57×10^8
	S_1–T_3	0.33	0.34	271.5	292.3	-419.4	2.51×10^7	2.5
Solid	S_1–T_1	0.19	0.39	52.1	24.5	47.7	4.81×10^7	2.68×10^7
	S_1–T_2	0.38	0.44	148.3	225.4	-146.5	2.00×10^5	1.30×10^8
	S_1–T_3	0.60	0.81	148.5	510.3	-146.5	3.47×10^4	4.40×10^8

SOC[a] based on the optimized single excited state structures respectively; SOC[b] based on the optimized triplet excited states structures respectively.

Particularly, in order to clearly express the rate, we calculate the effective K_{ISC} and K_{RISC} rates based on the following formulas:

$$K_{ISC}^{Cal}(S\rightarrow T)=\frac{K_{S_1-T_1}^2+K_{S_1-T_2}^2}{K_{S_1-T_1}+K_{S_1-T_2}}, \quad (3)$$

$$K_{RISC}^{Cal}(T\rightarrow S)=\frac{K_{T_1-S_1}^2+K_{T_2-S_1}^2}{K_{T_1-S_1}+K_{T_2-S_1}}. \quad (4)$$

The K_r, K_{ISC}^{Cal}, and K_{RISC}^{Cal} in the THF and solid phase are listed in Table 4. Compared with the solvent value, K_r in solid phase is increased by two orders of magnitude. The K_{ISC}^{Cal} (K_{RISC}^{Cal}) in the THF is 2.18×10^7 s^{-1} (1.81×10^{10} s^{-1}), and becomes 4.81×10^7 s^{-1}(2.68×10^7 s^{-1}) in the solid phase. It indicates that TADF phenomenon happens in both the THF and the solid phase. Although the TADF efficiency ($\Phi_{TADF}=\frac{\Phi_{ISC}\Phi_{RISC}}{1-\Phi_{ISC}\Phi_{RISC}}\Phi_{PF}$) depends both on the ISC efficiency ($\Phi_{ISC}=\frac{K_{ISC}}{K_r+K_{nr}+K_{ISC}}$, with K_{nr} the non-radiative rate) and the RISC efficiency ($\Phi_{RISC}=\frac{K_{RISC}}{K_{RISC}+K_{nrt}+K_{rt}}$, with K_{nrt} and K_{rt} the non-radiative rate and radiative rate of the triplet state), it has large dependence on the fluorescence efficiency ($\Phi_{PF}=\frac{K_r}{K_r+K_{nr}+K_{ISC}}$).[46] Based on the calculation results above, we can found that the fluorescent rates are significantly enhanced and the non-radiative process can be suppressed in aggregation, which can induce obviously enhanced fluorescent efficiency. That is also the reason that enhanced DF can be found in aggregation. In addition, the ratio of the delayed components was also increased in solid phase in experiment.[23] It should mainly depend on the ISC efficiency since the RISC efficiency should not be larger than the ISC efficiency due to the slower decay of the triplet states. The decreased non-radiative rate in solid state and increased ISC rate would be favor of the ISC efficiency.

Table 4. Calculated radiative rate (K_r), effective intersystem crossing rates (K_{ISC}^{Cal}), and effective reverse intersystem crossing rates (K_{RISC}^{Cal}).

	THF	Solid
K_r/s^{-1}	2.27×10^4	2.29×10^6
K_{ISC}^{Cal}/s^{-1}	2.18×10^7	4.79×10^7
K_{RISC}^{Cal}/s^{-1}	1.81×10^{10}	4.25×10^8

4. Conclusion

In summary, we comparatively investigated the photophysical processes for DMF-BP-DMAC in THF and solid phase using PCM and QM/MM methods respectively. Through analyzing the variation of the geometric parameters

and RMSD values of the molecules in both THF and solid phase, we found that the geometrical changes for molecule excitation in THF are much larger than those in solid phase. Due to the increase of the oscillator strength, the radiation rate in solid phase is nearly 100 times larger than that in THF. In addition, the HR factors are decreased in solid phase and they are mainly induced by the inhibition of the dihedral angle rotation. Therefore, the non-radiative channel in solid phase would be suppressed. The AIE property of the molecule should be induced by increased radiation rates and suppressed non-radiative process. Moreover, the small energy gap between S_1 and T_n as well as reasonable SOC and reorganization energy values cause efficient RISC rates in THF and solid phase. TADF phenomenon is confirmed in both THF and solid phase. Aggregation significantly influences both the ISC and RISC processes and more RISC channels are involved in solid state. The enhanced delayed fluorescence should be induced both by the enhanced fluorescent efficiency and ISC efficiency. Our calculations reasonably elaborate the experimental measurements, and help one to understand the AIDF mechanisms of DMF-BP-DMAC.

References

[1] Uoyama H, Goushi K, Shizu K, Nomura H and Adachi C 2012 *Nature* **492** 234

[2] Furukawa T, Nakanotani H, Inoue M and Adachi C 2015 *Sci. Rep.* **5** 8429

[3] Phelan G M 2018 *Inf. Disp.* **34** 10

[4] Komatsu R, Sasabe H, Seino Y, Nakao K and Kido J 2016 *J. Mater. Chem. C* **4** 2274

[5] Dias F B, Bourdakos K N, Jankus V, Moss K C, Kamtekar K T, Bhalla V, Santos J, Bryce M R and Monkman A P 2013 *Adv. Mater.* **25** 3707

[6] Zhang Y G, Zhang D D, Cai M H, Li Y L, Zhang D Q, Qiu Y and Duan L 2016 *Nanotechnology* **27** 094001

[7] Li X, Wang K, Shi Y Z, Zhang M, Dai G L, Liu W, Zheng C J, Ou X M and Zhang X H 2018 *J. Mater. Chem. C* **6** 9152

[8] Tanaka H, Shizu K, Miyazaki H and Adachi C 2012 *Chem. Commun.* **48** 11392

[9] Wang S P, Zhang Y W, Chen W P, Wei J B, Liu Y and Wang Y 2015 *Chem. Commun.* **51** 11972

[10] Xie G Z, Li X L, Chen D J, Wang Z H, Cai X Y, Chen D C, Li Y C, Liu K K, Cao Y and Su S J 2016 *Adv. Mater.* **28** 181

[11] Luo J, Xie Z, Lam J W, Cheng L, Chen H, Qiu C, Kwok H S, Zhan X, Liu Y and Zhu D 2001 *Chem. Commun.* **18** 1740

[12] Chen Y C, Lam J W Y, Kwok R T K, Liu B and Tang B Z 2019 *Mater. Horiz.* **6** 428

[13] Guo J J, Li X L, Nie H, Luo W W, Gan S F, Hu S M, Hu R R, Qin A J, Zhao Z J, Su S J and Tang B Z 2017 *Adv. Funct. Mater.* **27** 1606458

[14] Zhao Y D, Wang W G, Gui C, Fang L, Zhang X L, Wang S J, Chen S M, Shi H P and Tang B Z 2018 *J. Mater. Chem. C* **6** 2873

[15] Yang Z, Mao Z, Xu C, Chen X J, Zhao J, Yang Z Y, Zhang Y, Wu W, Jiao S B, Liu Y, Aldred M P and Chi Z G 2019 *Chem. Sci.* **10** 8129

[16] Guo J J, Fan J Z, Lin L L, Zeng J J, Liu H, Wang C K, Zhao Z J and Tang B Z 2019 *Adv. Sci.* **6** 1801629

[17] Guo J J, Zhao Z J and Tang B Z 2018 *Adv. Optical Mater.* **6** 1800264

[18] Zhang P P, Zeng J J, Guo J J, Zhen S J, Xiao B, Wang Z M, Zhao Z J and Tang B Z 2019 *Front. Chem.* **7** 199

[19] Zhang H K, Liu J K, Du L L, Ma C, Leung N L C, Niu Y L, Qin A J, Sun J Z, Peng Q, Sung H H Y, Williams I D, Kwok R T K, Lam J W Y, Wong K S, Phillips D L and Tang B Z 2019 *Mater. Chem. Front.* **3** 1143

[20] Yin X, Fan J Z, Liu J, Cai L, Sun H, Sun Y P, C K and Lin L L 2019 *Phys. Chem. Chem. Phys.* **21** 7288

[21] Fan J Z, Zhang Y C, Zhang K, Liu J, Jiang G Y, Li F Y, Lin L L and Wang C K 2019 *J. Mater. Chem. C* **7** 8874

[22] Huang J, Nie H, Zeng J J, Zhuang Z Y, Gan S F, Cai Y J, Guo J J, Su S J, Zhao Z J and Tang B Z 2017 *Angew. Chem. Int. Ed.* **56** 12971

[23] Zeng J J, Guo JJ, Liu H, Lam J W Y, Zhao Z J, Chen S M and Tang B Z 2019 *Chem-Asian J.* **14** 828

[24] Sun H T, Ryno S, Zhong C, Ravva M K, Sun Z R, Körzdörfer T and Brédas J L 2016 *J. Chem. Theory Comput.* **12** 2906

[25] Ruiz-Barragan S, Morokuma K and Blancafort L 2015 *J. Chem. Theory Comput.* **11** 1585

[26] Fan J Z, Zhang Y C, Zhang K, Liu J, Jiang G Y, Lin L L and Wang C K 2019 *Org. Electron.* **71** 113

[27] Lin L L, Fan J Z and Wang C K 2017 *Org. Electron.* **51** 349

[28] Cai L, Fan J Z, Kong X P, Lin L L and Wang C K 2017 *Chin. Phys. B* **26** 118503

[29] Ma H L, Peng Q, An Z F, Huang W and Shuai Z G 2019 *J. Am. Chem. Soc.* **141** 1010

[30] Wu Q Y, Zhang T, Peng Q, Wang D and Shuai Z G 2014 *Phys. Chem. Chem. Phys.* **16** 5545

[31] Frisch M J, Trucks G W, Schlegel H B, *et al.* 2016 *Gaussian 16* Rev. A.03, in, Wallingford, CT

[32] Lin L L, Fan J Z, Cai L and Wang C K 2018 *Mol. Phys.* **116** 19

[33] Cai L, Fan J Z, Lin L L and Wang C K 2017 *Mol. Phys.* **115** 809

[34] Lin L L, Wang Z J, Fan J Z and Wang C K 2017 *Org. Electron.* **41** 17

[35] Kong X P, Cai L, Fan J Z and Lin L L 2018 *Org. Electron.* **59** 7

[36] Fan J Z, Qiu S, Lin L L and Wang C K 2016 *Chinese J. Chem. Phys.* **29** 291

[37] Einstein A 1917 *Phys. Z.* **18** 121

[38] Vahtras O, Ågren H, Jo/rgensen P, Jensen H J r A, Helgaker T and Olsen J 1992 *J. Chem. Phys.* **97** 9178

[39] *Dalton, A Molecular Electronic Structure Program*

[40] Gao Y J, Chen W K, Zhang T T, Fang W H and Cui G 2018 *J. Phys. Chem. C* **122** 27608

[41] Lu T and Chen F W 2012 *J. Comput. Chem.* **33** 580

[42] Humphrey W, Dalke A and Schulten K 1996 *J. Molec. Graphics* **14** 33

[43] Chen R F, Tang Y T, Wan Y F, Chen T, Zheng C, Qi Y Y, Cheng Y F and Huang W 2017 *Sci. Rep.* **7** 6225

[44] Samanta P K, Kim D, Coropceanu V and Brédas J L 2017 *J. Am. Chem. Soc.* **139** 4042

[45] Reimers J R 2001 *J. Chem. Phys.* **115** 9103

[46] Tao Y, Yuan K, Chen T, Xu P, Li H H, Chen R F, Zheng C, Zhang L and Huang W 2014 *Adv. Mater.* **26** 7931